

# Prospects of solar axion searches with crystal detectors

S. Cebrián, E. García, D. González, I. G. Irastorza, A. Morales, J. Morales,  
A. Ortiz de Solórzano, J. Puimedón, A. Salinas, M. L. Sarsa, S. Scopel, J. A. Villar  
*Laboratorio de Física Nuclear. Universidad de Zaragoza*  
*50009, Zaragoza, SPAIN*

## Abstract

A calculation of the expected signal due to Primakoff coherent conversion of solar axions into photons via Bragg scattering in several crystal detectors is presented. The results are confronted with the experimental sensitivities of present and future experiments concluding that the sensitivity of crystal detectors does not challenge the globular cluster limit on the axion–photon coupling  $g_{a\gamma\gamma}$ . In particular, in the axion mass window  $m_a \gtrsim 0.03$  eV explored with this technique (not accessible at present by other methods)  $g_{a\gamma\gamma}$  might be constrained down to  $10^{-9}$  GeV $^{-1}$  (the recent helioseismological bound) provided that significant improvements in the parameters and performances of these detectors be achieved and large statistics accumulated. This bound should be considered as a minimal goal for the sensitivity of future crystal experiments. Consequently, finding a positive signal at this level of sensitivity would necessarily imply revisiting other more stringent astrophysical limits derived for the same range of  $m_a$  values.

*Key words:* dark matter; axions; Bragg scattering  
PACS: 95.35+d; 14.80.Mz; 61.10.Dp

## I. INTRODUCTION

Introduced twenty years ago as the Nambu–Goldstone boson of the Peccei–Quinn symmetry to explain in an elegant way CP conservation in QCD [1], the axion is remarkably also one of the best candidates to provide at least a fraction of the Dark Matter needed in Cosmology in order to explain both gravitational measurements and models of structure formation.

Axion phenomenology is determined by its mass  $m_a$  which in turn is fixed by the scale  $f_a$  of the Peccei–Quinn symmetry breaking,  $m_a \simeq 0.62 \text{ eV} (10^7 \text{ GeV}/f_a)$ . No hint is provided by theory about where the  $f_a$  scale should be. A combination of astrophysical and nuclear physics constraints, and the requirement that the axion relic abundance does not overclose the Universe, restricts the allowed range of viable axion masses into a relatively narrow window [2–4]:

$$\begin{aligned} 10^{-6} \text{ eV} &\lesssim m_a \lesssim 10^{-2} \text{ eV} \\ 3 \text{ eV} &\lesssim m_a \lesssim 20 \text{ eV}. \end{aligned} \tag{1}$$

The physical process used in axion search experiments is the Primakoff effect. It makes use of the coupling between the axion field  $\psi_a$  and the electromagnetic tensor:

$$\mathcal{L} = -\frac{1}{4} g_{a\gamma\gamma} \psi_a \epsilon_{\mu\nu\alpha\beta} F^{\mu\nu} F^{\alpha\beta} = -g_{a\gamma\gamma} \psi_a \vec{B} \cdot \vec{E} \tag{2}$$

and allows for the conversion of the axion into a photon.

Like all the other axion couplings,  $g_{a\gamma\gamma}$  is proportional to  $m_a$  [2,5]:

$$g_{a\gamma\gamma} \simeq 0.19 \frac{m_a}{\text{eV}} \left( \frac{E}{N} - \frac{2(4+z)}{3(1+z)} \right) 10^{-9} \text{ GeV}^{-1} \tag{3}$$

where  $E/N$  is the PQ symmetry anomaly and the second term in parenthesis is the chiral symmetry breaking correction. The anomaly  $E/N$  depends on the particular axion model, while the symmetry breaking correction is a function of the parameter  $z \equiv m_u/m_d \simeq 0.56$ . Two popular models are the GUT–DFSZ axion [6] ( $E/N=8/3$ ) and the KSVZ axion [7] ( $E/N=0$ ). However, it is possible to build viable axion models with different values of  $E/N$  [8] and the determination of the parameter  $z$  is subject to some theoretical uncertainties [9]. This implies that a very small or even vanishing  $g_{a\gamma\gamma}$  cannot be in principle excluded.

Solid state detectors provide a simple mechanism for axion detection [10,11]. Axions can pass in the proximity of the atomic nuclei of the crystal where the intense electric field can trigger their conversion into photons. In the process the energy of the outgoing photon is equal to that of the incoming axion.

Axions can be efficiently produced in the interior of the Sun by Primakoff conversion of the blackbody photons in the fluctuating electric field of the plasma. The resulting flux has an outgoing average axion energy  $E_a$  of about

4 keV (corresponding to the temperature in the core of the Sun,  $T \sim 10^7 K$ ) that can produce detectable x-rays in a crystal detector. Depending on the direction of the incoming axion flux with respect to the planes of the crystal lattice, a coherent effect can be produced when the Bragg condition is fulfilled, leading so to a strong enhancement of the signal. A correlation of the expected count-rate with the position of the Sun in the sky is a distinctive signature of the axion which can be used, at the least, to improve the signal/background ratio.

The process described above is independent on  $m_a$  and so are the achievable bounds for the axion-photon coupling  $g_{a\gamma\gamma}$ . This fact is particularly appealing, since other experimental techniques are limited to a more restricted mass range: “haloscopes” [12], that use electromagnetic cavities to look for the resonant conversion into microwaves of non relativistic cosmological dark halo axions, do not extend their search beyond  $m_a \simeq 50 \mu\text{eV}$ , while the dipole magnets used in “helioscope” [13] experiments are not sensitive at present to solar axions heavier than  $m_a \simeq 0.03 \text{ eV}$ .

A pilot experiment carried out by the SOLAX Collaboration [14] has already searched for axion Primakoff conversion in a germanium crystal of 1 kg obtaining the limit  $g_{a\gamma\gamma} \lesssim 2.7 \times 10^{-9} \text{ GeV}^{-1}$ . This is the (mass independent but solar model dependent) most stringent laboratory bound for the axion-photon coupling obtained so far, although less restrictive than the globular cluster bound [15]  $g_{a\gamma\gamma} \lesssim 0.6 \times 10^{-10} \text{ GeV}^{-1}$ . Notice however that the experimental accuracy of solar observations is orders of magnitude better than for any other star.

As a matter of fact, the solar model itself already requires [16]  $g_{a\gamma\gamma} \lesssim 10^{-9} \text{ GeV}^{-1}$ , whereas the above mentioned Ge experiment has not yet reached such sensitivity. The  $10^{-9} \text{ GeV}^{-1}$  limit sets, then, a minimal goal for the sensitivity of future experiments, prompting the need for a systematic discussion of present efforts and future prospects for axion searches with crystals. In the following we give the result of such an analysis, focusing on Germanium,  $\text{TeO}_2$  and NaI detectors.

## II. PRIMAKOFF CONVERSION IN CRYSTALS

We will make use of the calculation of the flux of solar axions of Ref. [17], with no direct coupling between the axion and the leptons (*hadronic axion*), with the modifications introduced in Ref. [11] to include helium and metal diffusion in the solar model. A useful parametrization of the flux is the following:

$$\frac{d\Phi}{dE_a} = \sqrt{\lambda} \frac{\Phi_0}{E_0} \frac{(E_a/E_0)^3}{e^{E_a/E_0} - 1} \quad (4)$$

where  $\lambda = (g_{a\gamma\gamma} \times 10^8 / \text{GeV}^{-1})^4$  is a dimensionless coupling introduced for later convenience,  $\Phi_0 = 5.95 \times 10^{14} \text{ cm}^{-2} \text{ sec}^{-1}$  and  $E_0 = 1.103 \text{ keV}$ .

The expected count-rate in a solid-state ionization detector, integrated in the electron-equivalent energy window  $E_1 < E_{ee} < E_2$ , is calculated starting from the expression:

$$R(E_1, E_2) = \int_{E_1}^{E_2} dE_{ee} \int_0^\infty dE_\gamma \frac{dR}{dE_\gamma}(E_\gamma) \frac{1}{\Delta\sqrt{2\pi}} e^{-\frac{(E_{ee}-E_\gamma)^2}{2\Delta^2}} \quad (5)$$

where  $E_\gamma$  is the energy of the outgoing photon,  $\Delta$  is the resolution of the detector, FWHM  $\simeq 2.35 \Delta$ , while:

$$\frac{dR}{dE_\gamma}(E_\gamma) = \int_0^\infty dE_a \frac{d\Phi}{dE_a}(E_a) \int d\Omega \frac{d\sigma}{d\Omega dE_\gamma}(E_\gamma). \quad (6)$$

$\sigma$  is the cross section of the process. The recoil of the nucleus can be neglected, so the energy of the outgoing photon is equal to that of the incoming axion and the differential cross section for the Primakoff conversion may be written as:

$$\frac{d\sigma}{dE_\gamma d\Omega} = \frac{d\sigma}{d\Omega} \delta(E_\gamma - E_a) \quad (7)$$

where [18]:

$$\frac{d\sigma}{d\Omega} = \frac{g_{a\gamma\gamma}^2}{16\pi^2} F_a^2(\vec{q}) \sin^2(2\theta). \quad (8)$$

$2\theta$  and is the scattering angle, while

$$F_a(\vec{q}) = k^2 \int d^3x \phi(\vec{x}) e^{i\vec{q}\cdot\vec{x}} \quad (9)$$

is the Fourier transform of the electrostatic field  $\phi$ .  $\vec{q}$  is the transferred momentum,  $q \equiv |\vec{q}| = 2k \sin \theta$  and  $k \equiv |\vec{k}| \simeq E_a$  is the axion momentum.

The energy distribution of Eq.(4) implies that  $q$  corresponds to a wavelength of a few Å, which is of the order of the distances between atoms in a typical crystal lattice. As a consequence of this a Bragg-reflection pattern arises in the calculation of the Fourier transform of Eq.(9) due to the periodic properties of the electric field in the crystal. Using translational invariance the periodic field may be written as [19] (we consider here the general case of a multi-target species):

$$\phi(\vec{x}) = \sum_{ij} \phi_{ij}(\vec{x}) = \sum_{ij} \frac{Z_j e}{4\pi|\vec{x} - \vec{x}_i|} e^{-\frac{|\vec{x} - \vec{x}_i|}{r_j}} = \sum_G n_G e^{i\vec{G}\cdot\vec{x}}. \quad (10)$$

where  $\vec{x}_i$  are the positions in space of the elements of the lattice,  $Z_j$  is the atomic number of the  $j$ -th type target nucleus,  $r_j$  is the screening length of the corresponding atomic electric field parametrized with a Yukawa-type potential, and the sum in the last term is intended over the vectors  $\vec{G}$  of the reciprocal lattice, defined by the property  $\exp i\vec{G}_i \cdot \vec{x}_i \equiv 1$ . A multi-target crystal is described by a Bragg lattice with a basis whose sites are occupied by atoms of different types. Indicating by  $a_i^j$  the  $i$ 'th basis vector occupied

by the  $j$ 'th target-nucleus type, the  $n_G$  coefficients appearing in Eq.(10) turn out to be:

$$n_G = \frac{1}{v_a} \sum_j S_j(\vec{G}) F_{a,j}^0(\vec{q} = \vec{G}) \quad (11)$$

where

$$S_j(\vec{G}) = \sum_i e^{i\vec{a}_i^j \vec{G}} \quad (12)$$

are the structure functions of the crystal and

$$F_{a,j}^0(\vec{q}) \equiv k^2 \int d^3x \phi_{ij}(\vec{x}) e^{i\vec{q} \cdot \vec{x}} = \frac{Z_j e k^2}{r_j^{-2} + q^2}. \quad (13)$$

is the form factor of Eq.(9) for a single  $j$ -type target.  $v_a$  indicates the volume of the elementary cell of the lattice.

Integration of Eqs.(5,6) over  $E_{ee}$  and  $E_a$  leads to:

$$R(E_1, E_2) = \int 2c \frac{d^3q}{q^2} \frac{d\Phi}{dE_a}(E_a) \frac{g_{a\gamma\gamma}^2}{16\pi^2} |F_a(\vec{q})|^2 \sin^2(2\theta) \mathcal{W} = \quad (14)$$

$$= (2\pi)^3 2c\hbar \frac{V}{v_a^2} \sum_G \frac{d\Phi}{dE_a}(E_a) \frac{1}{|\vec{G}|^2} \frac{g_{a\gamma\gamma}^2}{16\pi^2} \left| \sum_j F_{a,j}^0(\vec{G}) S_j(\vec{G}) \right|^2 \sin^2(2\theta) \mathcal{W} \quad (15)$$

where  $V$  is the volume of the detector,

$$\mathcal{W}(E_1, E_2, E_a, \Delta) = \frac{1}{2} \left[ \operatorname{erf} \left( \frac{E_a - E_1}{\sqrt{2}\Delta} \right) - \operatorname{erf} \left( \frac{E_a - E_2}{\sqrt{2}\Delta} \right) \right], \quad (16)$$

and in Eq.(14)  $|F_a(\vec{q})|^2$  has been expanded by making use of Eqs.(9,10,11,12). In the final result the integral over the transferred momentum has been replaced by a sum over the vectors of the reciprocal lattice, i.e. over the peaks that are produced when the Primakoff conversion verifies the Bragg condition  $\vec{q} = \vec{G}$  and the crystal interacts in a coherent way.

The Bragg condition implies that in Eq.(15)  $E_a = \hbar c \frac{|\vec{G}|^2}{2\hat{u} \cdot \vec{G}}$  where the unitary vector  $\hat{u}$  points toward the Sun. This term induces a time dependence in the expected signal.

### III. TIME CORRELATION AND BACKGROUND REJECTION

In the signal the dependence on  $\lambda$  can be factorized:  $R \equiv \lambda \bar{R}$ . An example of the function  $\bar{R}$  for several materials is shown in Fig. 1 as a function of time during one day and assuming the coordinates of the LNGS laboratory. The crystallographic inputs in the calculation are given in the Appendix. In all the plots the main axis of the lattice have been taken parallel to the South, West and upward directions. This explains the symmetry shown by all the plots.

The signal is peaked in energy around the maximum of the flux of Eq.(4) and presents a strong sub-diary dependence on time, due to the motion of the Sun in the sky. The time duration of the peaks decreases with growing energies, from tens of minutes in the lowest part of the axion energy window, down to a minimum of about one minute in the higher one, and is related to the energy resolution of each detector.

In order to extract the signal from the background for each energy interval  $E_k < E < E_k + \Delta E$  we introduce, following Ref. [14], the quantity:

$$\chi = \sum_{i=1}^n [\bar{R}(t_i) - \langle \bar{R} \rangle] \cdot n_i \equiv \sum_{i=1}^n W_i \cdot n_i \quad (17)$$

where the  $n_i$  indicate the number of measured events in the time bin  $t_i, t_i + \Delta t$  and the sum is over the total period  $T$  of data taking. Here and in the following the brackets indicate time average.

By definition the quantity  $\chi$  is expected to be compatible with zero in absence of a signal, while it weights positively the events recorded in coincidence with the expected peaks.

The time distribution of  $n_i$  is supposed to be given by a Poissonian with average:

$$\langle n_i \rangle = [\lambda \bar{R}(t_i) + b] \Delta t. \quad (18)$$

Assuming that the background  $b$  dominates over the signal the expected average and variance of  $\chi$  are given by:

$$\langle \chi \rangle = \lambda \cdot A \quad (19)$$

$$\sigma^2(\chi) \simeq b/A \quad (20)$$

with  $A \equiv \sum_i W_i^2 \Delta t$ . Each energy bin  $E_k, E_k + \Delta E$  with background  $b_k$  provides an independent estimate  $\lambda_k = \chi_k/A_k$  so that one can get the most probable combined value of  $\lambda$ :

$$\lambda = \frac{\sum_k \chi_k}{\sum_j A_j} \quad (21)$$

$$\sigma(\lambda) = \left( \sum_k A_k/b_k \right)^{-\frac{1}{2}}.$$

The sensitivity of an axion experimental search can be expressed as the upper bound of  $g_{a\gamma\gamma}$  which such experiment would provide from the non-appearance of the axion signal, for a given crystal, background and exposition. If  $\lambda$  is compatible to zero, then at the 95% C.L.  $\lambda \lesssim 2 \times 1.64 \times \sigma(\lambda)$ .

It is easy to see that the ensuing limit on the axion-photon coupling  $g_{a\gamma\gamma}^{lim}$  scales with the background  $b$  (assumed to be flat) and exposure  $MT$  in the following way:

$$g_{a\gamma\gamma} \leq g_{a\gamma\gamma}^{lim} \simeq K \left( \frac{b}{\text{cpd/kg/keV}} \times \frac{\text{kg}}{\text{M}} \times \frac{\text{years}}{\text{T}} \right)^{\frac{1}{8}} \times 10^{-9} \text{ GeV}^{-1} \quad (22)$$

where  $M$  is the detector mass and  $T$  the total time. The factor  $K \simeq 6.5 [\sum_k < (W(E_k)/M)^2 > \text{keV}/\Delta E_k]^{-1/8}$  is a function of the parameters of the crystal, as well as of the experimental threshold and resolution. The application of the statistical analysis described above results in a background rejection of about two orders of magnitude.

#### IV. DISCUSSION AND CONCLUSIONS

In order to perform a systematic analysis of the axion–detection capability of crystal detectors, we have applied the technique described in the previous section to several materials. The result is summarized in Table I, where the limit given by the experiment of Ref. [14] is compared to those attainable with running [20], being installed [21,22] and planned [23,24] crystal detector experiments.

In Table I a Pb detector is also included, to give an indication of the best improvement that one would expect by selecting heavy materials to take advantage of the proportionality to  $Z^2$  of the cross section of Eq.(8). These results can be easily extended to other elements with lower atomic numbers than those considered in Table 1 (for instance in  $\text{Al}_2\text{O}_3$  or LiF crystals, also in operation or planned dark matter experiments) although they are expected to yield less stringent limits.

In Fig.2 the result of our analysis is compared to the present astrophysical and experimental bounds in the plane  $m_a$ – $g_{a\gamma\gamma}$ . The horizontal thick line represents the constraint  $g_{a\gamma\gamma} \lesssim 3 \times 10^{-10} \text{ GeV}^{-1}$  taken from Table I. The mass intervals  $m_a \lesssim 10^{-6} \text{ eV}$ ,  $10^{-2} \text{ eV} \lesssim m_a \lesssim 3 \text{ eV}$ ,  $m_a \gtrsim 20 \text{ eV}$  are excluded respectively by cosmological overclosure [2], SN1987A [3] and oxygen excitation in water Cherenkov detectors [4], the edges of all the excluded regions being subject to many astrophysical and theoretical uncertainties. The horizontal lines represent the limits from SOLAX [14], helioseismology [16], and globular clusters [15]. The theoretical predictions for  $g_{a\gamma\gamma}$  in the case of the DFSZ and the KSFZ axion models are also given.

As shown in the expression of the  $g_{a\gamma\gamma}$  bound of Eq.(22), the improvement in background and accumulation of statistics is washed out by the 1/8 power dependence of  $g_{a\gamma\gamma}$  on such parameters. It is evident, then, that crystals have no realistic chances to challenge the globular cluster limit. A discovery of the axion by this technique would presumably imply either a systematic effect in the stellar–count observations in globular clusters or a substantial change in the theoretical models that describe the late–stage evolution of low–metallicity stars.

On the other hand, the sensitivity required for crystal–detectors in order to explore a range of  $g_{a\gamma\gamma}$ , compatible with the solar limit of Ref. [16], appears to be within reach, although only marginally, and provided that large improvements in background as well as substantial increase of statistics be guaranteed.

In light of the previous discussion, prospects to detect the axion with crystal detectors appear to be dim. The only realistic possibility to exploit this technique seems to rely on the fact that collecting a statistics of the order of a few tons $\times$ year could be achievable by adding properly the results of the various dark matter search experiments already planned for the near future. As shown in Fig.2 the ensuing limit for crystals would cross the theoretical models for an axion mass in the range of a few eV, in a region compatible with the bound given by SN1987A.

## APPENDIX

In this section we summarize the crystallographic information necessary to calculate the axion–photon coherent conversion discussed in section II for the materials shown in Table I. We recall that a Bravais lattice generated by the primitive vectors  $\vec{x}_i$  has a reciprocal lattice generated by the basis  $\vec{G}_i = 2\pi/v_a\epsilon_{ijk}\vec{x}_j \times \vec{x}_k$ , where  $v_a = \vec{x}_1 \cdot (\vec{x}_2 \times \vec{x}_3)$  is the volume of the primitive cell, while  $\epsilon_{ijk}$  is the totally anti–commutating tensor.

Germanium, sodium iodide and lead share the same type of underlying Bravais lattice, the faced–centered cubic crystal (fcc) structure generated by the primitive vectors [19]:

$$\begin{aligned}\vec{x}_1 &= \frac{a}{2}(0, 1, 1) \\ \vec{x}_2 &= \frac{a}{2}(1, 0, 1) \\ \vec{x}_3 &= \frac{a}{2}(1, 1, 0).\end{aligned}\tag{23}$$

The corresponding primitive cell sizes  $a$  are given in Table II, along with the basis vectors for Ge and NaI.

The Bravais lattice of TeO<sub>2</sub> is tetragonal. In the plots of Fig. 2 the longer side of the cell has been chosen in the vertical direction. In this case the generators are simply:

$$\begin{aligned}\vec{x}_1 &= a(1, 0, 0) \\ \vec{x}_2 &= a(0, 1, 0) \\ \vec{x}_3 &= b(0, 0, 1).\end{aligned}\tag{24}$$

with  $a=4.796 \text{ \AA}$  and  $b=7.626 \text{ \AA}$ . Each primitive cell contains a basis of 4 Tellurium atoms and 8 Oxygen atoms. Their positions in the primitive cell are given in Table III.

The parameter  $r_j$  entering the Yukawa potential of Eq.(10) is of the order of the atomic dimensions. In our calculation we have assumed  $r_j=1 \text{ \AA}$  for all the crystals. Varying  $r_j$  in the range  $0.5 \text{ \AA} \lesssim r_j \lesssim 1 \text{ \AA}$  affects the  $g_{a\gamma\gamma}$  limit by less than  $\simeq 30\%$ .



## ACKNOWLEDGEMENTS

This search has been partially supported by the Spanish Agency of Science and Technology (CICYT) under the grant AEN98-0627. One of us (S.S.) is supported by a fellowship of the INFN (Italy). The authors wish to thank Frank Avignone for useful discussions.

TABLES

TABLE I. Axion search sensitivities for running (DAMA [20]), being installed (CUORICINO [21], CANFRANC [22]) and planned (CUORE [23], GENIUS [24]) experiments are compared to the result of SOLAX [14]. To estimate the best improvement that would be possible by selecting high- $Z$  materials, a calculation is also shown for a Pb lattice, assuming the same conditions of background, threshold and resolution of the GENIUS experiment. The coefficient  $K$  has been introduced in Eq.(22).

	<b>K</b>	<b>M</b> (kg)	<b>b</b> (cpd/kg/keV)	$E_{th}$ (keV)	<b>FWHM</b> (keV)	$g_{a\gamma\gamma}^{lim}$ (2 years) (GeV $^{-1}$ )
<b>Ge</b> [14]	2.5	1	3	4	1	$2.7 \times 10^{-9}$
<b>Ge</b> [24]	2.5	1000	$1 \times 10^{-4}$	4	1	$3 \times 10^{-10}$
<b>TeO<sub>2</sub></b> [21]	3	42	0.1	5	2	$1.3 \times 10^{-9}$
<b>TeO<sub>2</sub></b> [23]	2.8	765	$1 \times 10^{-2}$	3	2	$6.3 \times 10^{-10}$
<b>NaI</b> [20]	2.7	87	1	2	2	$1.4 \times 10^{-9}$
<b>NaI</b> [22]	2.8	107	2	4	2	$1.6 \times 10^{-9}$
<b>Pb</b>	2.1	1000	$1 \times 10^{-4}$	4	1	$2.5 \times 10^{-10}$

TABLE II. Crystallographic information for Ge, NaI, and Pb:  $a$  is the primitive cell size and the  $\vec{a}_i^j$  are the basis vectors entering in the evaluation of the structure functions of Eq.(12).

<b>Species</b>	<b>a</b> (Å)	Basis $\vec{a}_i^j$
Ge	5.66	$\vec{a}_1^1 = (0,0,0)$ $\vec{a}_2^1 = \frac{a}{4}(1,1,1)$
NaI	6.47	$\vec{a}_1^1 = (0,0,0)$ (I) $\vec{a}_1^2 = \frac{a}{2}(1,1,1)$ (Na)
Pb	4.95	No basis

TABLE III. Basis vectors for TeO<sub>2</sub> entering in the evaluation of the structure function of Eq.(12). The longer side of the tetragonal primitive cell has been chosen in the vertical direction. All numbers are in Å.

<b>Oxygen</b>		<b>Tellurium</b>
$\vec{a}_1^1 = (0.998, 0.916, 1.480)$	$\vec{a}_2^1 = (3.797, 3.879, 5.293)$	$\vec{a}_1^2 = (0.093, 0.093, 0.000)$
$\vec{a}_3^1 = (1.481, 3.396, 3.386)$	$\vec{a}_4^1 = (3.314, 1.399, 7.199)$	$\vec{a}_2^2 = (4.702, 4.702, 3.813)$
$\vec{a}_5^1 = (1.399, 3.314, 0.426)$	$\vec{a}_6^1 = (3.396, 1.481, 4.239)$	$\vec{a}_3^2 = (2.304, 2.491, 1.906)$
$\vec{a}_7^1 = (0.916, 0.998, 6.145)$	$\vec{a}_8^1 = (3.879, 3.797, 2.332)$	$\vec{a}_4^2 = (2.491, 2.304, 5.719)$

## REFERENCES

- [1] R. D. Peccei and H. R. Quinn, *Phys. Rev. Lett.* **38** (1977) 1440.
- [2] E. W. Kolb and M. S. Turner, *The Early Universe*, Addison Wesley Publishing, (1990).
- [3] A. Burrows, M. T. Ressel and M. S. Turner, *Phys. Rev.* **D42** (1990) 3297.
- [4] J. Engel, D. Seckel and A. C. Hayes, *Phys. Rev. Lett.* **65** (1990) 960.
- [5] G. Raffelt, *Phys. Rep.* **198** (1990) 1.
- [6] M. Dine, W. Fischler and M. Srednicki, *Phys. Lett.* **B104** (1981) 199.
- [7] J. E. Kim, *Phys. Rev. Lett.* **43** (1979) 103; M. A. Shifman, A. I. Vainshtein and V. I. Zakharov, *Nucl. Phys.* **B166** (1980) 493.
- [8] J. E. Kim, *Phys. Rev.* **D58** (1998) 055006.
- [9] T. Moroi and H. Murayama, Berkeley University preprint UCB-PTH-98/20, hep-ph/9804291 (1998).
- [10] E. A. Paschos and K. Zioutas, *Phys. Lett.* **B323** (1994) 367.
- [11] R. J. Creswick, F. T. Avignone III, H. A. Farach, J. I. Collar, A. O. Gattone, S. Nussinov and K. Zioutas, *Phys. Lett.* **B427** (1998) 235.
- [12] C. Haggmann, D. Kinion, W. Stoeffl, K. van Bibber, E. Daw, H. Peng, L.J. Rosenberg, J. LaVeigne, P. Sikivie, N.S. Sullivan, D. Tanner, F. Nezirick, Michael S. Turner, D.M. Moltz, J. Powell and N.A. Golubev, *Phys. Rev. Lett.* **80** (1998) 2043; S. Matsuki, talk given at the II International Workshop on the Identification of Dark Matter (IDM98), Buxton, England, 7–11 September 1998.
- [13] S. Moriyama, M. Minowa, T. Namba, Y. Inoue, Y. Takasu and A. Yamamoto, *Phys. Lett.* **B434** (1998) 147.
- [14] A. O. Gattone, D. Abriola, F. T. Avignone, R. L. Brodzinski, J. I. Collar, R. J. Creswick, D. E. Di Gregorio, H. A. Farach, C. K. Guérard, F. Hasenbalg, H. Huck, H. S. Miley, A. Morales, J. Morales, S. Nussinov, A. Ortiz de Solórzano, J. H. Reeves, J. A. Villar and K. Zioutas (The SOLAX Collaboration), *Nucl. Phys.* **B(Proc. Suppl.)70** (1999) 59.
- [15] G. Raffelt, *Stars as Laboratories for Fundamental Physics* (University of Chicago Press, Chicago, 1996); G. Raffelt and D. Dearborn, *Phys. Rev.* **D36** (1987) 2211.
- [16] H. Schlattl, A. Weiss and G. Raffelt, submitted to *Astrop. Phys.*, hep-ph/9807476.
- [17] K. van Bibber, P.M. McIntyre, D.E. Morris and G. Raffelt, *Phys. Rev.* **D39** (1989) 2089.
- [18] W. Buchmüller and F. Hoogeveen, *Phys. Lett.* **B237** (1990) 278.
- [19] N. W. Ashcroft and N.D. Mermin, *Solid State Physics*, Saunders College, Philadelphia, 1976.
- [20] R. Bernabei, P. Belli, F. Montecchia, W. Di Nicolantonio, A. Incicchitti, D. Prospero, C. Bacci, C.J. Dai, L.K. Ding, H.H. Kuang and J.M. Ma, *Phys. Lett.* **B424** (1998) 195.
- [21] E. Fiorini, *private communication*; CUORICINO, *Letter of intent*, submitted to INFN and LNGS.
- [22] A. Morales, “Dark Matter and its Detection”, Summary Talk given at the NUPECC Workshop on Present and Future of Neutrino Physics, Frascati, *NUPECC Report in Highlights and Opportunities in Nuclear Physics*, Ed. by J. Vervier et al., December 1997, To be published in *Physics Reports*.
- [23] O. Cremonesi, Future of Cryogenic Detectors, talk given at NEUTRINO 98, Takayama, Japan, 4–9 June 1998, to be published in *Nucl. Phys.***B(Proc. Suppl.)1999**.
- [24] B. Majorovits, talk given at the II International Workshop on the Identification of Dark Matter (IDM98), Buxton, England, 7–11 September 1998.

## FIGURE CAPTIONS

**Figure 1** – Expected axion signals for Primakoff conversion in various crystals as a function of time for  $\lambda = 1$ . In the calculation the representative day of 1 april 1998 and the coordinates of the LNGS laboratory have been assumed. From top-left to bottom-right: a) Ge,  $2 \text{ keV} \leq E_{ee} \leq 2.5 \text{ keV}$ ; b) Ge,  $4 \text{ keV} \leq E_{ee} \leq 4.5 \text{ keV}$ ; c) TeO<sub>2</sub>,  $5 \text{ keV} \leq E_{ee} \leq 7 \text{ keV}$ ; d) TeO<sub>2</sub>,  $7 \text{ keV} \leq E_{ee} \leq 9 \text{ keV}$ ; e) NaI,  $2 \text{ keV} \leq E_{ee} \leq 4 \text{ keV}$ ; f) NaI,  $4 \text{ keV} \leq E_{ee} \leq 6 \text{ keV}$ .

**Figure 2** – The solar axion limit attainable with crystal detectors (horizontal thick line) is compared to the present astrophysical and experimental bounds and to the DFSZ and KSVZ axion theoretical predictions. The shaded mass intervals  $m_a \lesssim 10^{-6} \text{ eV}$ ,  $10^{-2} \text{ eV} \lesssim m_a \lesssim 3 \text{ eV}$ ,  $m_a \gtrsim 20 \text{ eV}$  are excluded respectively by cosmological overclosure [2], SN1987A [3] and oxygen excitation in water Cherenkov detectors [4]. The horizontal lines represent the upper limits for  $g_{a\gamma\gamma}$  from helioseismology [16] (dashes), SOLAX [14] (dots) and globular clusters [15] (dot-dashes). The regions excluded by haloscope searches [12] and the upper limit on  $g_{a\gamma\gamma}$  from the Tokio Helioscope experiment [13] are also shown.

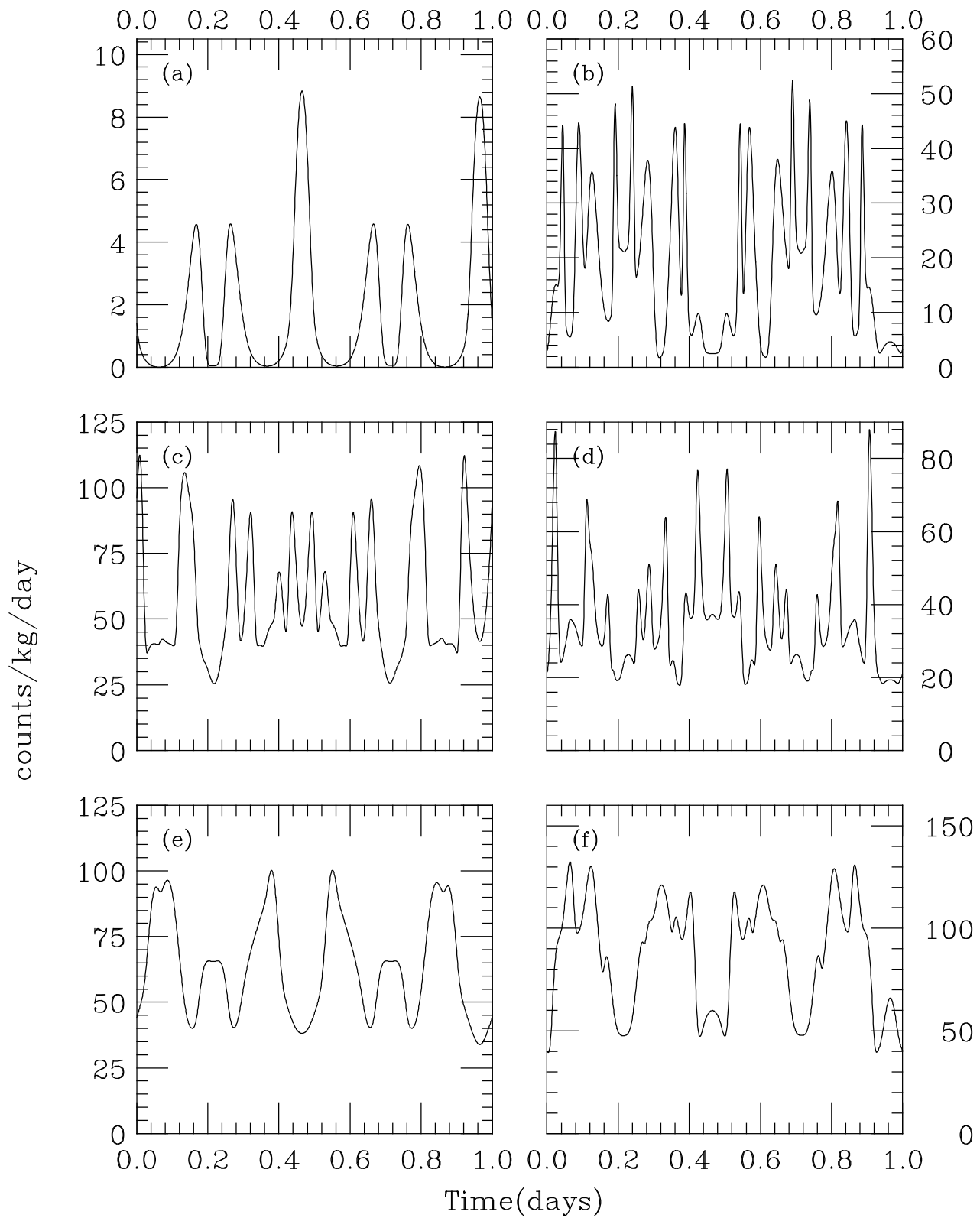


Figure 1

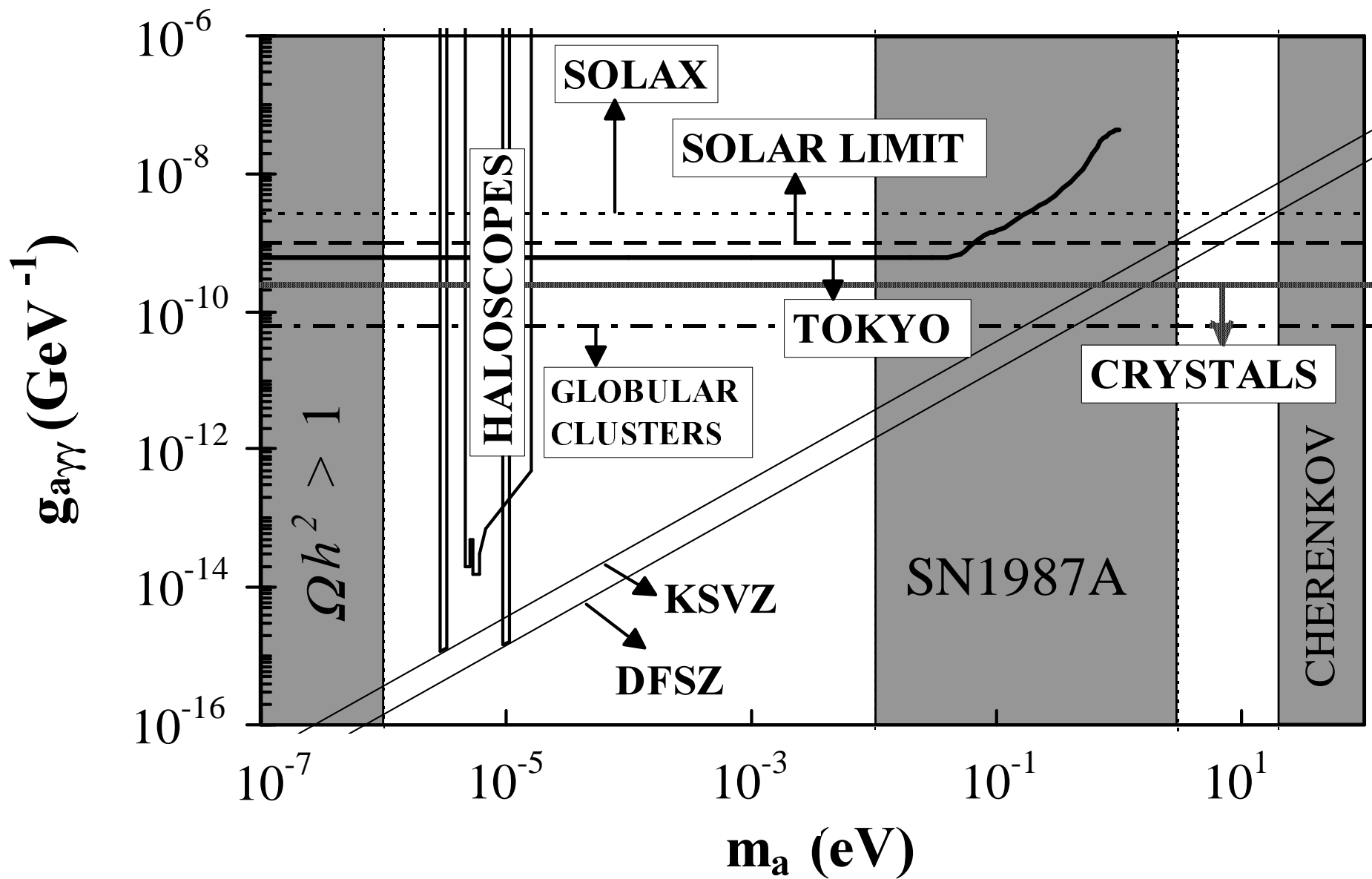


Figure 2